ARTICLE IN PRESS

Available online at www.sciencedirect.com

SCIENCE DIRECT

ELSEVIER

Nuclear Instruments and Methods in Physics Research A ▮ (▮▮▮▮) ▮▮▮–▮▮▮

NUCLEAR INSTRUMENTS & METHODS IN PHYSICS RESEARCH Section A

www.elsevier.com/locate/nima

Digital-sampling systems in high-resolution and wide dynamic-range energy measurements: Finite time window, baseline effects, and experimental tests

Luigi Bardelli*, Giacomo Poggi, NUCL-EX collaboration

I.N.F.N. and Department of Physics, University of Florence, Via G. Sansone 1, Sesto Fiorentino 50019, Italy

Received 5 August 2005; received in revised form 18 October 2005; accepted 2 December 2005

Abstract

Fast digital sampling and signal processing of the output of charge-sensitive preamplifiers connected to solid-state detectors, used in nuclear physics experiments, constitute effective replacements of the standard analog methods. If high-resolution and high-speed sampling Analog to Digital Converters (ADCs) are used, both the energy and timing resolution performances of the detector can be effectively exploited. The choice of a particular fast ADC in these applications is strictly related to the desired resolution and dynamic range of the system. In this paper a quantitative evaluation of system resolution is carried out—the results of [L. Bardelli and G. Poggi, Digital sampling-systems in high-resolution and wide dynamic-range energy measurements: comparison with peak sensing ADCs, this issue] are extended taking into account not only the detector noise, the digitizer properties, and the digital shaping, but also the use of a finite time interval for both baseline evaluation and digital shaping. The resulting performances are expressed using the parameter PSENOB [L. Bardelli, G. Poggi, Digital sampling-systems in high-resolution and wide dynamic-range energy measurements: comparison with peak sensing ADCs, this issue] and two additional correction terms. The effects due to ADC non-linearities are also briefly addressed. Simulations are presented to validate the proposed recipe. Experimental tests using a germanium detector in a wide dynamic-range configuration (at different counting rates) as well as an application to $\Delta E - E$ charged particle identification are shown. The presented discussion and results can be directly extended to various experimental arrangements.

PACS: 84.30.Sk; 07.50.Hp; 84.30.Vn; 29.40.Wk

Keywords: Baseline effects; Digital sampling; High-resolution energy measurements; Dynamic range; Semiconductor detectors

1. Introduction

High-resolution amplitude (i.e. energy) measurements are fundamental in various nuclear physics applications, as for example in γ spectroscopy measurements or charged particle detection/identification. In the last decade the availability of Analog to Digital Converters (ADCs) characterized by high-resolution (>10 bits) and sampling speed (>20 MSamples/s) has made it possible to use such systems as a replacement for standard analog electronics (i.e. analog shaping followed by peak-sensing converters), the main advantages being increased performances, flexibility, ease of maintenance, and generally lower costs.

In a commonly adopted configuration (as described for example in Ref. [1]) the digitizer is directly connected to the detector preamplifier output. The use of a proper signal processing of the data does not introduce any additional noise contribution, so that the highest Signal-to-Noise Ratio (SNR) can be achieved. Depending of the noise characteristics of the used detector/preamplifier configuration and of the experimental requirements (for example counting rate, ballistic deficit compensation with flat top filters, ...) an "optimal" digital filter can be synthetized (see for example Ref. [2] and references therein) and applied to the collected data in order to improve the SNR

*Corresponding author. Tel.: +39 055 4572693.
E-mail address: bardelli@fi.infn.it (L. Bardelli).

0168-9002/$ - see front matter © 2006 Elsevier B.V. All rights reserved.
doi:10.1016/j.nima.2005.12.250

and to extract the desired high-resolution amplitude information.

The properties of the used ADC, i.e. mainly the Effective Number of Bits and the sampling frequency, play a significant role to maintain the intrinsic detector amplitude resolution over a wide dynamic range. This point has been addressed in the companion paper [1], using very general hypotheses regarding the detection/ADC system under consideration. It has been shown that the digital system performances can be summarized by defining the quantity PSENOB, i.e. the "Peak-Sensing-Equivalent Number of Bits".

In Ref. [1] the practical problem of using a finite time interval (i.e. a finite number of samples) for digital signal shaping and the presence of a non-zero baseline value has been deliberately neglected. On the contrary, in this paper the resolution worsening due to both these effects is explicitly discussed and quantitatively evaluated. As a matter of fact, these topics have been decoupled from the first discussion [1] because the arising necessary complications would have made the presentation less perspicuous. The present paper shows that in most practical cases these effects can be kept sufficiently small so that the main results of Ref. [1] can still be applied.

The paper is organized as follows. After a brief presentation of the used event-based approach (Section 2), an exact computation of the attainable resolution is carried out (Section 3) for the general case of digital shaping, taking into account the baseline duration and the sampled preamplifier noise. The effects of the used baseline subtraction method for short baseline times are explicitly considered in Section 4, and a connection with the quantity PSENOB [1] is established. The used approach is validated in Section 5 using the simulation of a realistic wide dynamic-range experiment employing a germanium detector. ADC non-linearities are briefly addressed in Section 6. The discussion is also validated by experimental tests (Section 7) performed with a germanium detector (at various counting rates) and with a Si–CsI(Tl) telescope in a standard $\Delta E - E$ configuration using the AD conversion system described in Ref. [3].

2. Event-based and continuously running digital systems

In typical nuclear physics applications, for instance those requiring a large solid angle coverage, several detectors are often used, each of them typically provided with an independent electronic device for amplitude/energy measurement. Each of these measuring devices, either with analog or digital implementation, is usually based on two subsystems, one devoted to the very determination of the signal amplitude and the other one to the recognition of the presence of the signal. The first subsystem, referred to as "energy estimator" in the following, provides on demand an estimate of the amplitude/energy of the current event, by using proper filtering (thus also including any baseline correction, if needed). The second subsystem, "event-finder" in the following, provides a logic signal when a signal is present at the output of the associated detector. The "event-finder" output may also be used as a single channel trigger.

Using this schematization, the whole energy measurement process of a single detector consists in waiting for the event-finder subsystem to detect the presence of a signal of the detector, and then in transferring[1] the value provided by the energy estimator subsystem to the acquisition system.

Both subsystems can be implemented either with analog or digital methods. In a typical implementation using digital methods, the ADC is usually free-running, i.e. a digital data stream with fixed sampling period τ_{clk} is produced at any time. The details of the used event-finder system, either with a standard analog implementation (i.e. leading edge, constant fraction, ...) or a digital one as in Ref. [4], are immaterial for the following discussion and therefore will not be addressed in this paper.

Regardless of the implementation details, the event-finder subsystem must continuously check the input for detector events. On the other side, a digital implementation of the energy estimator subsystem may be realized either using an "event-based" or a "continuously running" configuration. The main difference between these two configurations resides in the way the digital data are on-line analysed by the energy estimator subsystem, resulting in different hardware and software requirements.

In event-based systems (as the one described in Ref. [3] and subsequent developments [5]) the energy estimation subsystem connected to the AD converter is usually in an idle state, waiting for the arrival of the logic signal from the event-finder subsystem. The digital data stream produced by the converter is thus normally ignored and no *real-time* digital signal processing is performed. When a detector signal is recognized by the event finder and the associated logic signal is produced, the energy estimation subsystem transfers into its memory the digital data belonging to the time window covering the signal of the current event, and starts the needed computations (including baseline corrections, if needed). A circular buffer is usually inserted between the AD converter and the processing system—old samples are discarded and new samples are stored in such a way that at each instant the last T_{BL}/τ_{clk} samples are available. The fired energy estimation subsystem is thus able to use a finite "baseline time" T_{BL} before the arrival of the detector signal.

In continuously running systems (as in the proposal [6,7]) the digital data stream coming from the AD converter is always fed into the energy estimation subsystem that performs a *real-time* implementation of the desired processing (including baseline corrections if

[1] In systems where many detectors are used and complex high-multiplicity events are of interest, an additional validation by a general "experiment" trigger is usually required, built on the various single channel triggers.

needed), with no hardware restriction on the available time window. When a detector event occurs, the measured energy value is already available (apart from a possibly non-zero fixed pipeline time delay), and is directly transferred to the acquisition system with no additional dead-time.

In the following sections an evaluation of the attainable energy resolution using a finite time window system is carried out, corresponding to the practical case either of an event-based energy estimator subsystem or of a continuously running system where the user has deliberately decided to limit the digital signal processing to a finite time window.

As far as the practical implementation details are concerned, the choice between the two configurations is fundamental in order to define the hardware and software requirements of the system and to characterize its dead-time.

As a matter of fact, continuously running systems are characterized by an ideally zero dead-time, and require an input/output and processing speed of the energy estimation subsystem high enough to withstand the output data rate of the AD converter. Depending of the AD converter used, this may severely restrict the available choices of the hardware for real-time processing. For example if a ~100 MSamples/s converter is used (as in Refs. [3,8,9] or in the proposals [6,7]), only fast FPGAs would be feasible, ruling out all of the today available DSP processors on the market. It has to be noted also that the typical processing time required by a modern fast FPGA to perform a sum between two 16 bit operands is of the order of 8–20 ns, i.e. comparable or longer than the typical sampling period of high-speed ADCs. This means that a non-trivial FPGA-based implementation is required to withstand the ADC throughput rate.

On the other side, an event-based system is characterized by a higher dead-time, corresponding to the time needed by the energy estimation subsystem to perform the computation of the signal amplitude after each event. Due to the fact that the digital data stream can be stored on fast temporary memory for later retrieval, event-based systems can afford the use of both FPGAs and DSPs as energy estimation subsystems. DSPs, while usually not as fast as FPGAs, allow the use of much more sophisticated algorithms that can be easily coded and maintained, taking full advantage of the flexibility of these processors.

An example of an event-based system using a DSP-based energy estimator and a simple analog event-finder system is the prototype board described in Ref. [3], with the developments of Ref. [5], that we have developed. This system has been designed in order to be versatile enough to be applied to several detector types (silicon, CsI, fast scintillators, gas avalanche counters [9,10]) normally used in nuclear reaction studies at Fermi energies [11–16]. Besides, these experiments usually require from a few hundreds to thousands of electronic sampling channels. The typical reaction-events of interest involve a multiplicity of fired detectors significantly higher than unity, and the typically involved reaction-event counting-rates are of the order of 1 kcps. For each of the used detectors, several physical quantities (energy, timing, pulse-shape, ...) are needed, and thus an event-based, DSP-equipped system has been chosen to implement the energy-, timing-, and pulse-shape-estimators. In these applications, due to the relatively non-demanding counting-rate requirements, and a fortiori in future applications in Radioactive Nuclear Beam facilities, the DSP-related dead-time is not an issue.

3. Energy resolution with finite-time-window shaping and baseline subtraction

In the present and the following sections we calculate the energy resolution when a finite time window is used for performing digital shaping (for example in the previously discussed event-based systems). The calculation also includes the issue of baseline evaluation and subtraction, that is well known to be very important for high-resolution wide-dynamic-range energy measurements. After this preliminary discussion, in the following sections the influence of ADC Effective Number of Bits and sampling rate is quantitatively investigated exploiting the conclusions of this section. The formalism adopted in the following derivations coincides, where possible, with the notations used in Ref. [1].

A correct baseline evaluation usually requires a "baseline time" T_{BL} free from detector events (or from long decaying tails of the preceding ones). All the baseline-relevant information is extracted from the available T_{BL}/τ_{clk} samples preceding the rise of the signal. In Fig. 1 a typical output of a charge preamplifier over a relatively long time scale is shown. Two distinct events can easily be seen, together with the corresponding time windows used by an event-based system (supposed to have $T_{BL} = 4\,\mu s$ as in

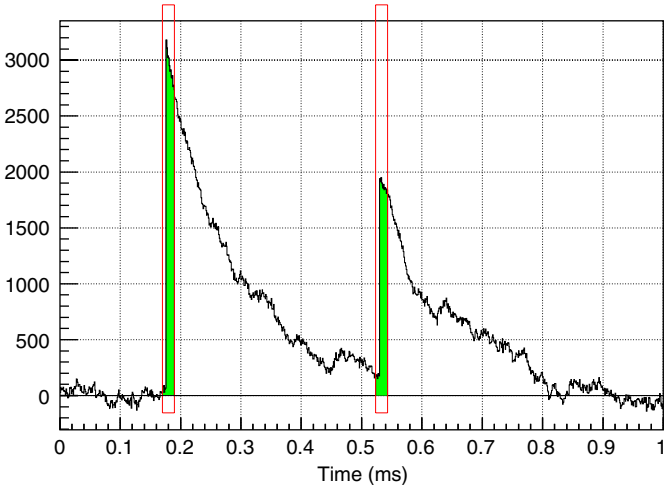

Fig. 1. Example of the output of a charge preamplifier over a long time scale. Two distinct events can easily be seen. The shaded areas correspond to the time windows available to an event-based system.

Ref. [5] and a total measuring time limited to 20 μs). Given the long time base shown in Fig. 1, the main features of the preamplifier fluctuations are associated to the low frequency step noise. In practical situations pick-up and interferences from the environment, for instance 50/60 Hz noise related to the power lines, can also be present. Detector dark current, preamplifier-output offset, and poor pole-zero cancellation or AC coupling associated with high counting-rate, may contribute with additional DC components. These DC/low-frequency components constitute the baseline which the signal develops over. In Fig. 2 an example of an acquired digital sequence is presented. The waveform from the considered event-based system starts at the time conventionally chosen as $t = 0$ in the figure, and a finite time T_{BL} precedes the rise of the detector signal. This is the only time-window used for the whole procedure of baseline evaluation/subtraction and digital shaping.

In the literature, many papers deal with the problem of baseline subtraction for high resolution energy measurements, both using analog baseline restorers (as pioneered by Radeka [17]) and digital filtering [18]. As far as digital baseline-restores are concerned, in the approach of Ref. [18] any baseline shift is described as an equivalent detector dark current I_{eq} and therefore the baseline determination consists in the evaluation of I_{eq}. To this aim, the procedure can be schematized as applying a proper weight function to the detector current signal obtained by digital deconvolution of the preamplifier response—the optimal weight function can be determined starting from the known noise sources at the detector level.

In this work a different approach has been chosen, similar to the one proposed few years ago in Ref. [19]. The baseline is evaluated at the preamplifier level as an average of the available samples preceding the signal and subtracted. The resulting preamplifier signal is then digitally shaped starting from $t = 0$. The proposed method does not need any detailed knowledge of the preamplifier response, and it can be directly applied to several experimental configurations, providing spectroscopy-grade resolutions and dynamic ranges (as it will be shown later). This method performs at the same time the baseline evaluation over a finite time interval and the digital shaping over a finite number of samples. For this reason, in the following "finite baseline time" and "finite time window" are used as synonyms. The connection of this procedure with the formalism of Ref. [18] is reported in Appendix A.

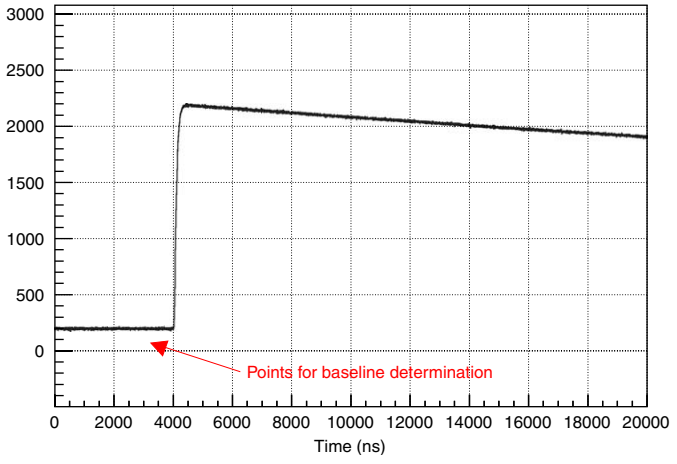

Fig. 2. Example of digitized event for an event-based analysis. Note the very different time scale with respect to the one used in Fig. 1.

As anticipated, for each event the baseline is estimated as an average of the N_{BL} ($N_{BL} = T_{BL}/\tau_{clk}$) samples available in the first portion of the signal:

$$BL = \frac{1}{N_{BL}} \sum_{i=1}^{N_{BL}} S[i]. \tag{1}$$

The obtained BL value is then subtracted from the whole sequence $S[k]$, and a digital shaping filter is applied.

A quantitative computation of the noise properties of the system is performed, taking into account the baseline subtraction. This computation cannot be performed in the frequency domain because the acquired sequence $S[k]$ is non-stationary, since $S[k] = 0$ for $t < 0$. The evaluation must be carried out in the time domain.

Given the preamplifier response $P[k]$ to a δ-like detector current ($P[k] = 0 \ \forall k < 0$, having for example a step-like shape with exponential decay), the signal $S'[k]$ after baseline subtraction can be decomposed into signal and noise components:

$$S'[k] = S[k] - BL; \quad S[k] = q \cdot P[k - N_{BL}] + n[k] \tag{2}$$

where $q \cdot P$ is the noiseless preamplifier signal to be measured, q is the deposited charge in the detector, and $n[k]$ describes the noise/DC components. With this notation, the subtracted BL value is thus given by

$$BL = \frac{1}{N_{BL}} \sum_{i=1}^{N_{BL}} n[i]. \tag{3}$$

For a noisy preamplifier with an ideal zero DC offset in the output, $n[k]$ (and thus BL) has zero expectation value (over an ensemble of events). When a non-zero offset (possibly slowly varying) is present, the baseline subtraction method (Eq. (2)) allows for a compensation of this effect. As a matter of fact, no hypothesis on the $n[k]$ expectation value $\langle n \rangle$ is required for the following computations.

The output of the digital filter is computed with a convolution between $S'[k]$ and the digital filter response to a δ-like signal, that will be denoted by $G[k]$ (the notation $G(t)$ will be used for its continuous-time equivalent). It has to be noted that G includes all the necessary features for a proper amplitude measurement, for example pole-zero cancellation and ballistic deficit compensation. The integral of $G(t)$ will be denoted with $G_{int}(t)$, coinciding with the filter output to a perfect step input.

With reference to Fig. 3, the overall energy fluctuation (in shaper output units[2]) can be computed as the variance

[2]In order to obtain the resolution in preamplifier output units or for comparison between different filters having different gains, a normalization factor equal to $[G_{int}(T_M)]^2$ must be applied in Eq. (4).

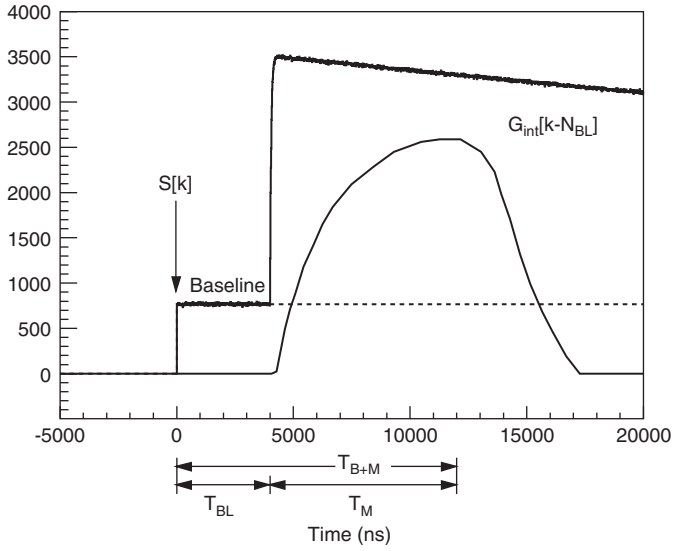

Fig. 3. Definition of the quantities used in the text. The signal $S[k]$ has been acquired with a finite T_{BL} ($T_{\mathrm{BL}} = 4\,\mu\mathrm{s}$ in the figure).

of the shaped signal at the measuring time T_{M}, as defined in Ref. [1] (where the signal starts at time = 0). Usually T_{M} is chosen as the time when the output of the digital filter reaches its maximum. With the used notation, the resulting shaped signal reaches its maximum at time $T_{\mathrm{B+M}} = T_{\mathrm{BL}} + T_{\mathrm{M}}$ (see Fig. 3).

One immediately verifies that the expectation value of the output of the digital filter is given by $qP * G$ ("$*$" denotes the convolution), i.e. the noise expectation value $\langle n\rangle$ cancels out. For the variance $\sigma^2(T_{\mathrm{B+M}})$ of the output of the digital filter at $T_{\mathrm{B+M}}$ the following expression is obtained:

$$\sigma^2(T_{\mathrm{B+M}}) = \mathbb{E}_e\left\{\left(\sum_{h=1}^{N_{\mathrm{B+M}}} (n[h] - \mathrm{BL}) \cdot G[N_{\mathrm{B+M}} - h]\right)^2\right\} \tag{4}$$

where $N_{\mathrm{B+M}} = T_{\mathrm{B+M}}/\tau_{\mathrm{clk}}$ and the notation $\mathbb{E}_e\{\xi\}$ indicates the expectation value of the quantity ξ over an ensemble of events. The noisy samples $n[k]$ are supposed to be described as a stationary random process. The autocorrelation function $\mathscr{R}(\theta)$ of $n[k]$ is defined as usual:

$$\mathscr{R}(\theta) = \lim_{T\to\infty} \frac{1}{2T}\int_{-T}^{T} [n(t) - \langle n\rangle][n(t+\theta) - \langle n\rangle]\,\mathrm{d}t. \tag{5}$$

The quantity BL in Eq. (4) is not a constant but rather a value extracted from the noisy samples $n[k]$ for $1 \leqslant k \leqslant N_{\mathrm{BL}}$ (see Eq. (3)) and therefore various autocorrelation-like terms ($n[k]\cdot n[h]$) appear in the expansion of Eq. (4).

Carrying on the calculations in the discrete time domain as already discussed in the derivation of [1, Eq. (5)], one obtains

$$\begin{aligned}\sigma^2(T_{\mathrm{B+M}}) = {} & \sum_{k,h=1}^{N_{\mathrm{B+M}}} G[N_{\mathrm{B+M}} - k]G[N_{\mathrm{B+M}} - h]\cdot \mathbb{E}_t\{n[k]n[h]\} \\ & + \frac{1}{N_{\mathrm{BL}}^2}\left(\sum_{k,h=1}^{N_{\mathrm{B+M}}} G[N_{\mathrm{B+M}} - k]G[N_{\mathrm{B+M}} - h]\right) \\ & \times\left(\sum_{i,j=1}^{N_{\mathrm{BL}}} \mathbb{E}_t\{n[i]n[j]\}\right) \\ & - \frac{2}{N_{\mathrm{BL}}}\sum_{k,h=1}^{N_{\mathrm{B+M}}}\sum_{i=1}^{N_{\mathrm{BL}}} G[N_{\mathrm{B+M}} - k]G[N_{\mathrm{B+M}} - h] \\ & \times \mathbb{E}_t\{n[k]n[i]\}.\end{aligned} \tag{6}$$

From Eq. (6) it can be easily seen that the possibly non-zero average noise value $\langle n\rangle$ cancels out, as expected, regardless of the used filter G and T_{BL} time interval. This means that any DC component at the output of the preamplifier is removed by the outlined procedure (an alternative proof is given in Appendix A). Passing to continuous variables and using the given definition of the noise autocorrelation function, the obtained energy resolution reads

$$\begin{aligned}\sigma^2(T_{\mathrm{B+M}}) = {} & \underbrace{\iint_{x,y=0}^{T_{\mathrm{B+M}}} G(T_{\mathrm{B+M}} - x)G(T_{\mathrm{B+M}} - y)\mathscr{R}(x-y)\,\mathrm{d}x\,\mathrm{d}y}_{①} \\ & + \frac{1}{T_{\mathrm{BL}}^2}\underbrace{\left[\int_{x=0}^{T_{\mathrm{B+M}}} G(T_{\mathrm{B+M}} - x)\,\mathrm{d}x\right]}_{②} \\ & \times \underbrace{\left[\iint_{x,y=0}^{T_{\mathrm{BL}}} \mathscr{R}(x-y)\,\mathrm{d}x\,\mathrm{d}y\right]}_{③} \\ & - \frac{2}{T_{\mathrm{BL}}}\left[\int_{x=0}^{T_{\mathrm{B+M}}} G(T_{\mathrm{B+M}} - x)\,\mathrm{d}x\right] \\ & \times \underbrace{\left[\int_{x=0}^{T_{\mathrm{B+M}}} \mathrm{d}x\int_{y=0}^{T_{\mathrm{BL}}} \mathrm{d}y\, G(T_{\mathrm{B+M}} - x)\mathscr{R}(x-y)\right]}_{④}\end{aligned} \tag{7}$$

The term ① is the contribution due to the use of the finite time window $T_{\mathrm{B+M}}$ for digital shaping, whereas the terms ②, ③ and ④ are associated with the baseline subtraction algorithm. The ADC noise can be easily included in Eq. (7) by adding to the detector autocorrelation function $\mathscr{R}(\theta)$ an ADC-related autocorrelation term $b_{\mathrm{ADC}} f_S/2\cdot\delta(\theta)$. Eq. (7) can be applied once the autocorrelation function $\mathscr{R}(\theta)$ is known, typically with a dedicated measurement of the sampled noise at the output of the preamplifier. Eq. (7) gives an analytical expression of the overall energy resolution for any given shaping filter $G(t)$ and noise

spectral density, taking into account the availability of a finite baseline and shaping time.

In the limit $T_{BL} \to \infty$ only the term ① of Eq. (7) survives, i.e. the special case of infinite number of samples available for shaping and zero baseline is obtained. This exactly corresponds to [1, Eq. (5)], that is the limit of Eq. (7) for $T_{BL} \to \infty$.

In the following sections a quantitative evaluation of the general formula Eq. (7) is performed for realistic experimental configurations.

4. PSENOB and effects of the baseline subtraction for finite T_{BL}

In this section the resolution loss due to the use of a finite length baseline will be considered and a connection to the quantity PSENOB defined in Ref. [1] is established.

In the same hypotheses used in Ref. [1, Section 3], the overall system energy resolution $\sigma_{exp,BL}$ with a given ADC and using a finite baseline time can be computed from Eq. (7). In analogy with Ref. [1], grouping the non-white and white terms and including the σ_p^2 and σ_D^2 contributions, one obtains

$$\sigma_{exp,BL}^2 = H_G^2(T_{BL}) + (b + b_{ADC})k_G^2(T_{BL}) + \sigma_p^2 + \sigma_D^2 \qquad (8)$$

where the same notation of Ref. [1, Eq. (6)] has been used and the ADC noise, neglecting time-jitter effects [1], is denoted by b_{ADC} (given in Ref. [1, Eq. (2)]). The two terms $H_G(T_{BL})$ and $k_G(T_{BL})$ obviously depend on the used digital filter and baseline time. Using the explicit expression for the term $k_G(T_{BL})$ (given in Appendix B) it is seen that it converges to the k_G term defined in Ref. [1, Eq. (7)] in the limit $T_{BL} \to \infty$. With a slight abuse of notation, in the following this limit (i.e. the k_G term of Ref. [1, Eq. (7)]) will be denoted with $k_G(\infty)$, and similarly for H_G.

For a given filter G, we define $\sigma_{th,BL=\infty}$ as the theoretically achievable resolution with an infinite baseline time in the chosen experimental conditions, i.e. in the ideal situation where no contribution arises from the digitizer system—$\sigma_{th,BL=\infty}^2 = H_G^2(\infty) + bk_G^2(\infty) + \sigma_p^2 + \sigma_D^2$.

The ratio between $\sigma_{exp,BL}^2$ and $\sigma_{th,BL=\infty}^2$ is

$$\frac{\sigma_{exp,BL}^2}{\sigma_{th,BL=\infty}^2} = \left[\frac{H_G^2(T_{BL}) + bk_G^2(T_{BL}) + \sigma_p^2 + \sigma_D^2}{H_G^2(\infty) + bk_G^2(\infty) + \sigma_p^2 + \sigma_D^2}\right] + \left[\frac{k_G^2(T_{BL})b_{ADC}}{\sigma_{th,BL=\infty}^2}\right]. \qquad (9)$$

Recalling the definition of PSENOB, given in Ref. [1, Eq. (9)], two quantities λ'_{BL} and ρ_{BL} can be defined so that the first addendum of Eq. (9) is given by $[1 + \lambda'_{BL}]$ and the full equation can be written as

$$\frac{\sigma_{exp,BL}^2}{\sigma_{th,BL=\infty}^2} = 1 + \lambda'_{BL} + (1 + \rho_{BL})\frac{9}{12}\left(\frac{R}{3\sigma_{th,BL=\infty}}\right)^2 \cdot \frac{1}{4^{PSENOB}}. \qquad (10)$$

With respect to the original equations using PSENOB [1, Eq. (8)], two correction terms are present:

λ'_{BL} *term*. This term is directly related to the baseline subtraction algorithm, and it does not depend on the chosen AD converter. This reflects the loss of information due to the use of a finite baseline time that would be present also if a noiseless ADC (i.e. very large PSENOB value) were used. In the limit $T_{BL} \to \infty$ we obtain $\lambda'_{BL} = 0$.

ρ_{BL} *term*. This term increases the importance of the ADC noise contribution (i.e. the PSENOB-related term) taking into account the evaluation of the baseline over the finite T_{BL} time. In the limit $T_{BL} \to \infty$ we obtain $\rho_{BL} = 0$.

It has to be noted that, as shown in Eq. (10), neither λ'_{BL} nor ρ_{BL} include any ADC-related parameter (i.e. ENOB or f_S), and therefore they can be computed once the detector/preamplifier noise, the used digital filter, and the available baseline time are known. PSENOB is thus the only quantity in Eq. (10) that depends on the ADC characteristics.

Eq. (10) can be used to predict the attainable resolution in a given experimental condition, once the two terms $H_G(T_{BL})$ and $k_G(T_{BL})$ are known. In practical cases, these two terms can be numerically calculated using Eq. (7) once the detector noise autocorrelation function $\mathscr{R}(\theta)$ has been measured and the white noise component (which appears as a δ-like contribution in $\mathscr{R}$) is separated from the non-white one.

In order to quantitatively evaluate the importance of the two correction terms, the special important case of a solid-state detector/charge-sensitive preamplifier is examined. The detector spectral noise density is assumed to have the "standard" expression $a/\omega^2 + b$ (the same case has been also discussed in Ref. [1, Section 4]). We consider shaping filters typically employed in energy measurements with solid-state detectors (i.e. triangular, trapezoidal, CR-RC^n). We further assume that the shaping time parameter of each filter has been optimized in order to achieve the maximum resolution with the used detector in infinite baseline operating conditions. With this hypothesis the electronic resolution is given by $2k_G(\infty)b$.

As discussed in Ref. [1, Section 4], these filters can be represented by the expression $G(t) = 1/\vartheta \cdot G^\star(t/\vartheta)$ (i.e. Ref. [1, Eq. (10)]), using as scaling parameter ϑ the optimal detector corner time (see the discussion of Ref. [1, Table 1]). Substituting in Eq. (8), one obtains ($x_{BL} = T_{BL}/\tau_C$):

$$\sigma_{exp,BL}^2 = a\tau_C h_{G\star}^2(x_{BL}) + \frac{b + b_{ADC}}{\tau_C} k_{G\star}^2(x_{BL}) + \sigma_p^2 + \sigma_D^2. \qquad (11)$$

The expressions for $h_{G\star}(x_{BL})$ and $k_{G\star}(x_{BL})$ (defined in analogy with Ref. [1]) are given in Appendix B. In the limit $x_{BL} \to \infty$, these two terms are closely related to the "step noise index" and "delta noise index" as defined in Ref. [20].

Substituting in Eqs. (9) and (10) one obtains

$$\lambda'_{\mathrm{BL}} = \frac{k^2_{G\star}(x_{\mathrm{BL}}) + h^2_{G\star}(x_{\mathrm{BL}}) - 2k^2_{G\star}(\infty)}{2k^2_{G\star}(\infty)} \cdot \eta = \lambda_{\mathrm{BL}} \cdot \eta \qquad (12)$$

$$\rho_{\mathrm{BL}} = \frac{k^2_{G\star}(x_{\mathrm{BL}}) - k^2_{G\star}(\infty)}{k^2_{G\star}(\infty)}. \qquad (13)$$

The quantity η is the square of the ratio between the electronic resolution and the overall resolution (i.e. including σ_p^2 and σ_D^2). As already discussed in Ref. [1, Section 3], when only electronic resolutions are of concern σ_p^2 and σ_D^2 are removed and $\eta = 1$.

The two quantities λ_{BL} and ρ_{BL} have been computed for various representative filters. As evident from the explicit expressions of $k^2_{G\star}(x_{\mathrm{BL}})$ and $h^2_{G\star}(x_{\mathrm{BL}})$ (and well known in the literature, see for example Ref. [18]), the parameter x_{BL} may be used as scaling parameter when the performances of these different filters are compared. The results are reported in Fig. 4 as a function of x_{BL}.

For finite width filters (i.e. triangular and trapezoidal ones) the two correction terms λ_{BL} and ρ_{BL} are exactly zero as soon as the baseline is evaluated over a time greater than the total filter width. Therefore, for these filters, it is possible to reach the theoretical resolution limit by using a finite baseline time. This is not the case for infinite width filters (i.e. CR-RC^4 and infinite cusp), the infinite cusp being the most sensitive to baseline effects.

Fig. 4 allows for a quantitative estimate of the importance of baseline-related effects on the final energy resolution. From the figure it is apparent that a digital-sampling system, once the digital shaping includes a baseline subtraction evaluated over $T_{\mathrm{BL}} \sim 1$–$2\tau_{\mathrm{C}}$, is able to practically reach the theoretically maximum resolution of the used AD converter/shaping filter (i.e. $\lambda_{\mathrm{BL}}, \rho_{\mathrm{BL}} \ll 1$). These quantitative results, although obtained using a different baseline subtraction method, are in fair agreement with the discussion on the baseline time given for a particular case in Ref. [18]. For low x_{BL} values the resolution is dominated by the white-noise component,

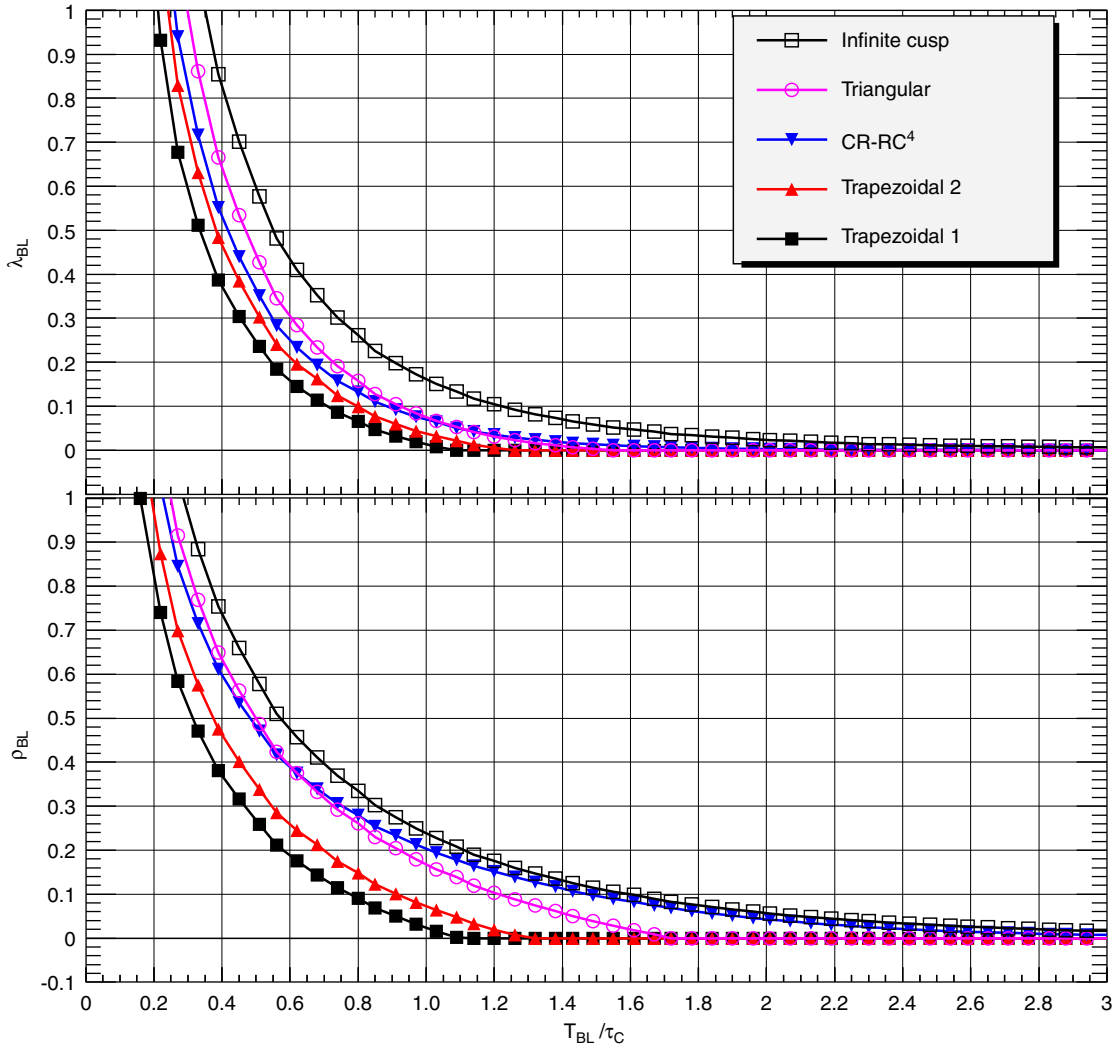

Fig. 4. Results of a numerical evaluation of the two parameters λ_{BL} and ρ_{BL} for various filter types. "Trapezoidal 1" is a trapezoidal filter with a flat top time equal to the linear rise time, whereas in "Trapezoidal 2" the flat top time is half the rise time. See text for details.

given the nearly exact elimination of the low-frequency noise operated by the baseline subtraction method.

As anticipated, the presented discussion has been carried out in the low counting-rate limit, i.e. without significant preceding signals tails over the considered T_{BL} time. As experimentally verified and reported in Section 7.1, these results can be safely applied even in presence of a significant counting rate, once the standard prescription of a fast preamplifier decay time with proper pole-zero compensation is used. This solution is well known to be very effective in removing the influence of preceding signals tails, thus allowing a moderate sensitivity to counting rate.

5. Comparison with simulations

In this section the previously discussed results are validated by a simulation. The simulation allows to explore a wide range of AD converter characteristics (ENOB and f_S) for various choices of baseline times once an experimental setup is defined. Experimental tests are reported in Section 7.

A typical germanium-based detection system for high-resolution γ ray experiments has been considered. The simulated detector–preamplifier system is characterized by its performances under an ideal shaping, i.e. an electronic resolution $\sigma_{th,BL=\infty} = 0.3$ keV using a CR-RC^4 filter with optimal shaping time constant $\tau_{sha,opt} = 3\,\mu s$. The system noise is assumed to have a spectral noise density $a/\omega^2 + b$, and then $\tau_{sha,opt} = \sqrt{b/7a}$. The CR-RC^4 digital filter has been considered for the sake of simplicity and ease of comparison with standard analog systems. Moreover, as discussed in Section 4, this digital filter exhibits a sizeable sensitivity to baseline-effects, and allows for a more stringent test of the calculation.

In the simulation, a proper noise contribution is added to the signals, which are digitized and processed by a simulated digital system running at various sampling speeds, using a baseline subtraction algorithm followed by digital CR-RC^4 shaping with a shaping time of 3 μs (no further τ_{sha} optimization as a function of b_{ADC} and T_{BL} has been performed). A full range $R = 10$ MeV has been used (compatible with the requirements of experiments with 4π γ arrays like Refs. [6,7]). About 1000 events for each point have been used for determining the simulated energy resolutions.

In Figs. 5 and 6 the simulation results are compared with the predictions of Eq. (10) for $T_{BL} = 1$ and 4 μs, respectively, whereas Fig. 7 refers to the case of infinite baseline time. In each figure the points marked with the ■ symbol represent the simulation results, while the predictions of Eq. (10) are shown as continuous curves. The digital shaping energy resolution is shown as a function of the ENOB of the converter. The integer number of "physical" bits B has been chosen as $\mathtt{int}(\mathrm{ENOB}) + 2$, i.e. $B = 12$ for ENOB = 10.8, according to the typical characteristics of commercial ADCs. In each figure the predicted performances for four different sampling speeds (50/100/200 MSamples/s, 1 GSample/s) are shown also (as a reference, a typical digital oscilloscope is characterized by 1 GSample/s, 7 effective bits). On the right of the figures the equivalent dynamic range of the system is reported, defined as the ratio between the full range (i.e. 10 MeV in the figures) and 3σ, i.e. we assume that only signals greater than three times the resolution are detectable.

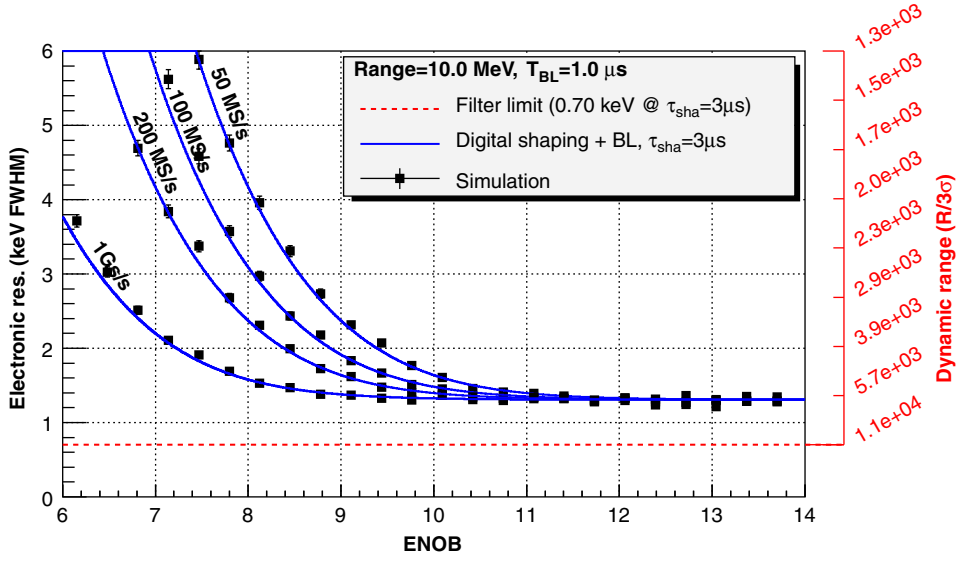

Fig. 5. Digital electronic energy resolution from Eq. (10) using a simple CR-RC^4 equivalent digital shaping filter as a function of the effective number of bits of the converter and considering a baseline time $T_{BL} = 1$ μs. The resolution is evaluated also for various ADC sampling frequencies. A comparison between the detailed simulation presented in the text and the predictions of Eq. (10) (continuous curves) is included. The equivalent dynamic range, defined as $R/3\sigma$, is shown on vertical axis on the right side of the figure.

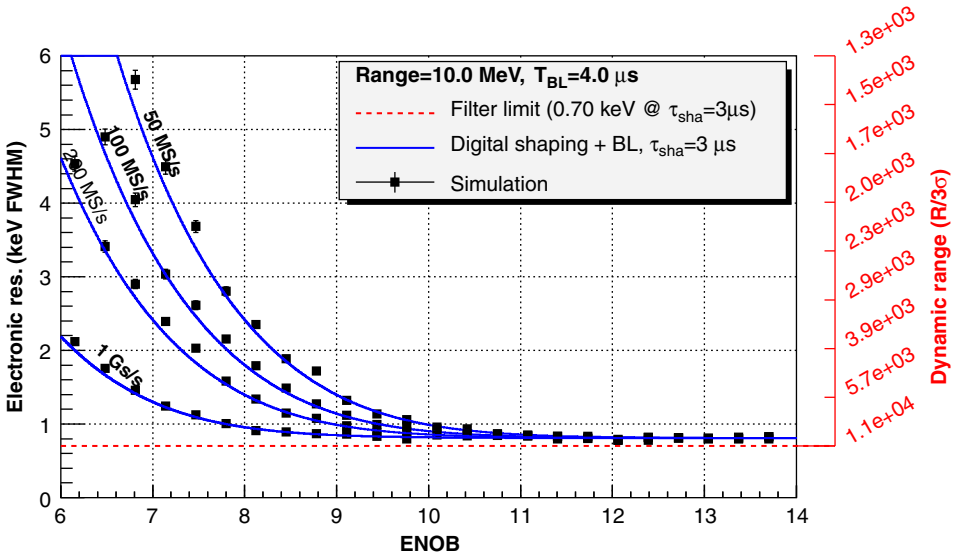

Fig. 6. Same as Fig. 5, but using a baseline time $T_{BL} = 4\,\mu s$.

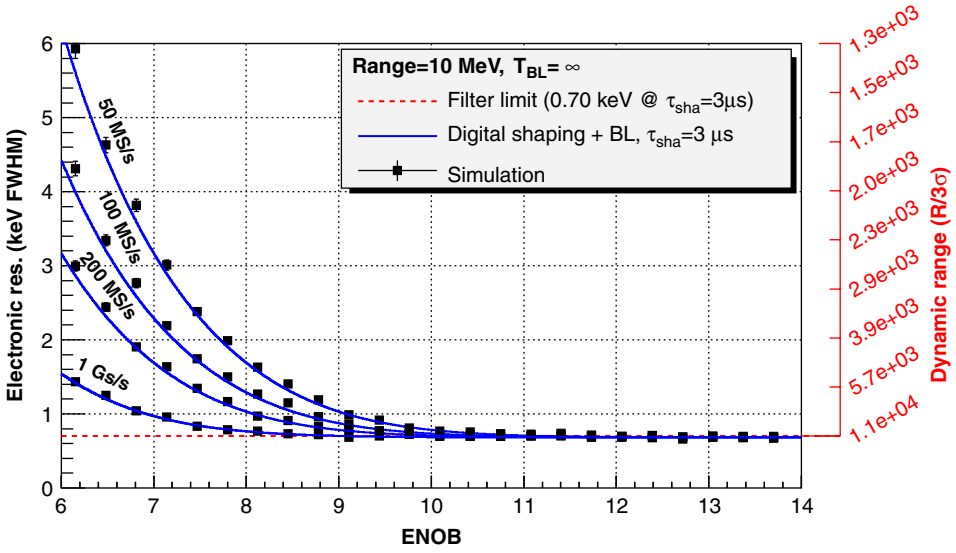

Fig. 7. Same as Fig. 5, but using an infinite baseline time T_{BL}.

From the figures a very good agreement between the simulated points and the prediction of Eq. (10) is evident for the explored range of converter resolutions, sampling speeds, and T_{BL} times. These results validate the approach proposed in Ref. [1] with the additional correction terms of Section 4, summarized by the three key parameters PSENOB (the only term depending on the ADC properties), λ_{BL} e ρ_{BL} (baseline only terms). For finite baseline times (Figs. 5 and 6) and very high PSENOB values, only the term λ_{BL} influences the achievable electronic resolution. On the other side, the data reported in Fig. 7, being characterized by $\lambda_{BL} = \rho_{BL} = 0$, can be directly obtained from Ref. [1, Fig. 1].

There is an appreciable discrepancy at low values of ENOB, where the simulated points are characterized by a worse resolution than the predicted ones. In fact, the hypotheses used for the evaluation of the sampling noise are accurate only when the quantization noise is smaller than the noise at the ADC analog input. For low-resolution converters this assumption is no longer valid (no dithering [21] occurs) and thus a discrepancy with respect to the predicted value is indeed observed in the expected direction.

6. Non-linearity effects

In the previous discussion as well as in Ref. [1] the contribution to the finally attainable energy resolution and dynamic range due to ADC non-linearities (either of the AD converter or of its analog front end) has been

Table 1
Results of a numerical simulation including ADC integral non-linearity

Integral non-linearity (LSB)	Resolution (keV FWHM)
0	0.806
0.5	0.814
1	0.817
1.5	0.818
2	0.82
3	0.83
4	0.86
5	0.89

Data refer to a 10.8 effective bits, 100 MSamples/s converter in the same simulated experimental condition of Fig. 6. See text for details.

neglected, whereas pile-up effects and a fluctuating baseline in presence of a significant non-linearity may influence the final resolution.

To quantitatively estimate the importance of these effects, the simulation described in the previous section has been modified in order to include a non-zero integral non-linearity of the digitizer. Data have been simulated for the case of a 12 bit (10.8 effective) 100 MSamples/s converter, using a 4 μs T_{BL} time and taking into account various degrees of non-linearity of the system (assumed having a second-order polynomial behaviour). The obtained results are shown in Table 1 for a baseline fluctuation of ~20 keV FWHM (compatible with the experimental test of Section 7.1).

In the first column of the table the used integral non-linearities are shown, defined as the maximum deviation from the best linear fit over the full converter range. As a reference, typical values for a 12 bit ADC microchip (i.e. without considering the analog front end) are in the 0.2–1 LSB range. In the second column the obtained simulated resolutions are shown. These values do not include any systematic contribution (the peak shift due to the non-linearity of the system), i.e. only the statistical fluctuations around the obtained peak centroid are considered. From the table one does not see any significant contribution to the overall resolution as soon as the non-linearity is smaller than ~1 LSBs. Additional analysis of the simulated data confirms indeed that the main source of resolution worsening can be traced back to baseline fluctuations that explore a not negligible portion of the full converter range. From this discussion it follows that as long as the non-linearity of the used digitizer (ADC and analog front end) is limited to ~1 LSB its effect on the attainable resolution and dynamic range is negligible.

An off-line non-linearity measurement of the AD converter is anyway advisable when characterizing the setup. If needed, this information can be stored in a look-up table and effectively used during data taking for on-line correction of the digitized samples, for instance when the non-linearity itself is sizeably larger or when significantly high baseline fluctuations (or pile-up) are present.

By modifying the simulation in order to include the differential non-linearity (typical value: ±0.5 LSB), we verified that no significant resolution worsening is introduced. This is due to the beneficial sliding-scale-like effects intrinsically included in the amplitude measurements, due both to the asynchronous sampling of the decaying preamplifier signal [22] and to the baseline fluctuations.

7. Experimental tests

In order to test the energy resolution properties of a digital-sampling system, experimental tests have been carried out using the prototype digitizing system of Ref. [3], i.e. a 12 bit 100 MSamples/s digitizer. The effective number of bits of the used converted has been measured at various input frequencies (1–10 MHz) using an Anritsu 68147C sinusoidal generator, with an additional quartz filtering to reduce the oscillator phase noise. The obtained data are consistent with 10.8 effective bits for the used ADC, the time-jitter contributions being zero within errors. The integral non-linearity of the system has been measured to be 0.8 bits (using the same definition of Section 6).

7.1. Experimental test with a germanium detector

An experimental test with a 30% efficiency coaxial germanium detector has been carried out, using a ^{60}Co source. The preamplifier output of the detector, having a 57 μs decay time, is directly coupled to the digitizer. A maximum baseline time $T_{BL} = 10\,\mu s$ has been used.

The full range of the AD converter in this test was about 14 MeV. The achieved resolution (using a digital CR-RC^4 filter with $\tau_{sha} = 2\,\mu s$) on the 1.3 MeV line is 2.1 keV FWHM, where the resolution of an injected pulser signal is 1.1 keV FWHM. From independent measurements the maximum electronic resolution for this detector–preamplifier system is indeed known to be 1.1 keV FWHM. The measurements were performed at a counting rate of ~1 kcps.

In order to evaluate the performances of the system as a function of the baseline time, the collected events have been processed using only a fraction of the available baseline time. The results are shown (with symbols) in Fig. 8, for both the 1.3 MeV ^{60}Co line and the injected pulser. A detailed comparison with the prediction of Eq. (7) can be performed by numerically extracting the autocorrelation function $\mathcal{R}(\theta)$ of the overall system noise from the experimental digitized dataset and by direct computation of Eq. (7). The results are shown, with lines, in Fig. 8 (the prediction for the 1.3 MeV line is obtained by adding the statistical fluctuations to the electronic resolution). A good agreement between the experimental data and the prediction of Eq. (7) is evident.

Using the prescriptions of Ref. [1] and of Section 4, the considered case corresponds to a corner time constant of ~5 μs, and to a PSENOB value of ~15. For the case T_{BL}~10 μs the λ_{BL} and ρ_{BL} effects can be neglected

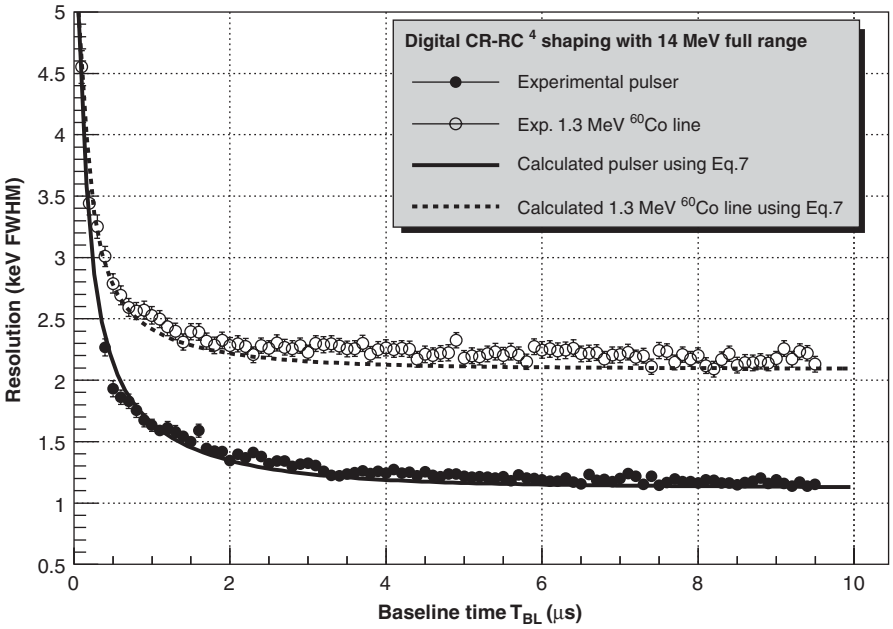

Fig. 8. Resolution as a function of the available baseline time, using baseline subtraction and a CR-RC^4 digital filter. Symbols: experimental data. Lines: prediction of Eq. (7) using an experimentally determined $\mathscr{R}(\theta)$. The pulser resolution using a standard analog system was about 1.1 keV FWHM.

($T_{BL}/\tau_C \simeq 2$, see Fig. 4), and thus the system resolution can also be extracted from Ref. [1, Fig. 1]. In the shorter baseline-time cases, the numerical evaluation of Eq. (7) with the experimental $\mathscr{R}(\theta)$, as in Fig. 8, is needed only when a very precise prediction is required. However, since in many practical case the detector noise can be safely approximated with $a/\omega^2 + b$, the formulæ and results of Section 4 can be satisfactorily applied ($<5\%$ error on the average for the electronic resolution data in Fig. 8).

In order to check the sensitivity of the used shaping and baseline subtraction algorithms to pile-up effects, the measurements have been repeated for various counting rates. The standard procedure of using a faster decaying preamplifier has been used, i.e. a CR network with pole-zero compensation has been inserted to reduce the preamplifier decay time from the original value (57 μs) to 3.5 μs. The very same analysis has been performed on the collected data for counting rates ranging from 1 up to 20 kcps. With no event selection, an electronic resolution worsening of about 0.2 keV at the maximum examined counting rate has been observed. If the same analysis is performed but for a shorter shaping time ($\tau_{sha} \sim 1$ μs), a resolution worsening of only 0.05 keV is observed over the used counting-rate range. The use of a digital deconvolution of the preamplifier response did not show any resolution improvement.

7.2. Test with a $\Delta E - E$ Silicon–CsI(Tl) telescope

A test has been also performed for a configuration widely used in charged particle experiments, namely a Silicon–CsI(Tl) telescope. This well known setup employs a $\Delta E - E$ identification method to measure not only the energy but also the charge (and the mass) of the incoming particles. The identification power is limited by the ΔE detector characteristics (as the thickness uniformity), energy straggling, and—to a much lesser extent—by the electronic resolution on the silicon channel.

In Refs. [9,23] the aforementioned digitizer has been used to sample the Si and the CsI signals and to build a $\Delta E - E$ identification plot (Fig. 1 of Ref. [9]). The experimental arrangement used a 300 μm thick, 2 cm^2 Si detector and a 3 cm thick CsI(Tl) with photodiode readout. The full range on the digitizer on the Si channel is about 500 MeV. Both preamplifiers have a silicon-equivalent noise of about ~60 keV FWHM. Due to hardware restrictions, the available baseline time in the test was only about 200 ns.

In order to test the presented computation the experimental dataset (where the waveforms corresponding to each event were stored on disk) has been re-processed to simulate a wider dynamic range. The originally acquired waveforms are first scaled to comply with the increased dynamic range. A proper white noise contribution (corresponding to 10.8 effective bits over the simulated range) is afterward added, and the samples are re-quantized with 12 bit resolution. This procedure allows to simulate the performances of the used digitizer (10.8 ENOB) as if a wider dynamic range were used in the test. The obtained waveforms have then been processed with a baseline subtraction followed by digital CR-RC^4 shaping (0.7 μs), and the $\Delta E - E$ plots corresponding to the new ranges have been produced. Each $\Delta E - E$ correlation has been linearized in order to extract a particle identification (P.I) spectrum. In Fig. 9 the corresponding plots are shown.

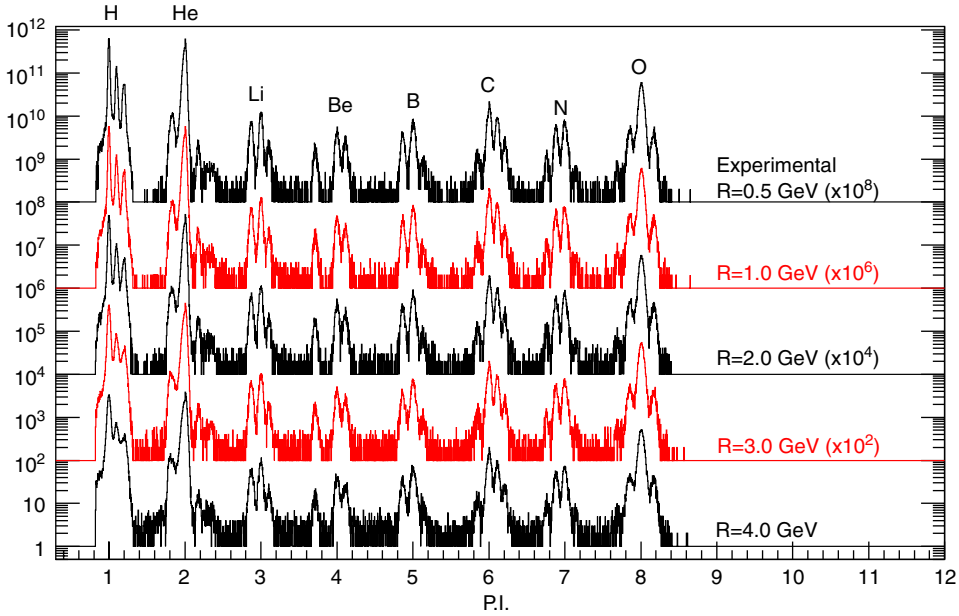

Fig. 9. Particle identification (P.I) spectra obtained for various dynamic ranges. The experimental data, collected with range R = 500 MeV, have been reprocessed in order to simulate wider dynamic ranges.

Table 2
Quantitative evaluation of the particle identification performances for various simulated ranges

Range (MeV)	$p \leftrightarrow d$ from Eq. (10)	$p \leftrightarrow d$	$d \leftrightarrow t$	$^3He \leftrightarrow ^4He$	$^4He \leftrightarrow ^5He$	$^5Li \leftrightarrow ^6Li$	$^7Be \leftrightarrow ^9Be$	$^9Be \leftrightarrow ^{10}Be$	$^9B \leftrightarrow ^{10}B$	$^{12}C \leftrightarrow ^{13}C$	$^{13}N \leftrightarrow ^{14}N$	$^{15}O \leftrightarrow ^{16}O$
Exp.: 500	1.80	1.82	1.38	1.37	1.90	1.34	2.44	0.91	1.15	0.96	0.95	1.04
1000	1.68	1.67	1.27	1.35	1.88	1.29	2.40	0.88	1.11	0.96	0.95	1.01
1500	1.51	1.50	1.15	1.30	1.83	1.30	2.37	0.86	1.14	0.94	0.96	1.03
2000	1.33	1.34	1.03	1.22	1.77	1.24	2.45	0.90	1.14	0.92	0.98	1.01
2500	1.18	1.14	0.86	1.17	1.46	1.22	2.21	0.82	1.04	0.91	0.91	0.96
3000	1.03	1.02	0.77	1.10	1.53	1.13	2.07	0.85	1.00	0.89	0.89	0.92
3500	0.94	0.91	0.70	1.05	1.32	1.12	1.96	0.81	1.01	0.86	0.88	0.87
4000	0.85	0.81	0.62	0.94	1.36	1.06	1.90	0.71	0.95	0.84	0.88	0.82

The obtained Factor of Merit (FoM) is reported for various nuclei pairs. The experimental data have been collected using a 500 MeV range. In the second column estimated FoM values obtained from Eq. (10) are reported.

It is possible to appreciate the presence of a full isotopic identification for all the particles produced in the used reaction ($^{16}O+^{116}Sn$, beam energy of 250 MeV). When wider dynamic ranges are used, the attained identification capabilities seen in the 500 MeV range are maintained for $Z \gtrsim 2$ and only degrade gracefully for hydrogen isotopes. The isotopic resolution is thus available up to the maximum considered range of 4 GeV. As quantitatively shown shortly, the digital system dynamic range would have been even larger if a longer baseline time were used, as we plan to do in future experiments [5].

The resulting dynamic range is at least a wide as the ones obtained by heavy ion experiments like INDRA [11] or CHIMERA [16]. As a matter of fact, these two experiments, based on standard analog shaping techniques (with final digitization performed with QDCs or peak-sensing ADCs), are forced to use a double electronic chain with different gains (high/low) to cover the needed dynamic range.

A quantitative measurement of the attained identification capabilities as a function of the simulated range can be performed using the Factor of Merit (FoM) as defined in Ref. [24], i.e. the ratio between the two peaks distance and the sum of the two FWHM resolutions. The results for several nuclei pair are shown in Table 2.

It is possible to see that the FoM values for $Z \gtrsim 2$ undergo only a minor deterioration, whereas a somewhat greater effect is present for $Z = 1$.

A quantitative comparison between the data in Table 2 and Eq. (10) over the full particle and energy range is difficult because of the presence of many experimental effects, not known with sufficient accuracy, that influence

the P.I. FoM computation (for example detector inhomogeneities and/or energy straggling as a function of particle type and energy).

For the case of the $p \leftrightarrow d$ FoM a semiquantitative comparison can be performed, estimating a proton energy straggling of about 180 keV FWHM from the Bohr stopping formula. Since the other experimental effects are expected to be small, this is the major non-electronic contribution. The system performances can be predicted using Eq. (10), with $\tau_C = 1.9\,\mu s$ and PSENOB $\simeq 14.4$. Since $T_{BL}/\tau_C \simeq 0.1$, the corresponding values for λ_{BL} e ρ_{BL}, assuming the standard $a/\omega^2 + b$ noise behaviour, are 3.3 and 1.8, respectively (outside the range of Fig. 4). Since the experimental resolution is mainly determined by the detection mechanism, the evaluation of Eq. (10) is performed using these parameters and explicitly taking into account the σ_D^2 contribution due to energy straggling. The parameter η (Eq. (12)) is 0.1. One obtains an expected energy resolution ranging from 220 keV FWHM with 500 MeV ADC full range, up to 300 keV FWHM with 4 GeV full range. Given the average separation energy between p and d of about 1.3 MeV, a "predicted" FoM value can be estimated for each energy range shown in Table 2; this estimate is reported in the second column of Table 2. The maximum deviation from the "simulated" FoM is less than 5%.

From the presented discussion is evident that the 12 bit (10.8 ENOB) converter can be employed in experiments requiring isotopic P.I from $Z = 1$ upwards, with a full energy range of few GeVs. It has to be noted that, if a longer baseline were used (for example 4 μs as planned in Ref. [5]), the predicted resolution at 4 GeV full range would be 230 keV FWHM ($\lambda_{BL}, \rho_{BL} \ll 1$ for $T_{BL}/\tau_C \simeq 2$), a very tiny increase with respect to the low-range value. This result confirms once again that, once the described signal processing method includes a baseline time of the order of twice the detector noise corner time, the only parameter controlling the digital sampling and shaping contribution to the resolution is PSENOB, and therefore the results of Ref. [1] directly apply.

In order to reach these performances, the use of wide dynamic-range preamplifier and a high uniformity ΔE detector is mandatory, whereas a moderate preamplifier resolution (~100 keV) can be tolerated. A differential preamplifier output (and differential ADC input) is expected to be necessary in order to reduce pick-up noise.

Identification spectra with poorer resolution than the ones shown in Fig. 9 have been reported in the recent work [25] using a 14 bit 105 MSamples/s ADC. A discrepancy with the theoretical and experimental results shown in this work using a 12 bit, 100 MSamples/s ADC is evident. Assuming proper preamplifier performances, clean cabling and good choice of the various digital processing parameters in Ref. [25], the apparent performance difference is probably due to non-optimal detector behaviour.

8. Conclusions

In this paper an extensive evaluation of the limiting factors influencing energy measurements with sampling ADCs has been carried out, starting from the conclusions of the companion paper [1]. An expression for the attainable resolution has been presented for the general case of a sampling system employing digital shaping over a finite time, having a finite baseline-time preceding the arrival of the event, taking into account the ADC effective number of bits and the presence of any preamplifier noise. The resulting formulæ have been re-expressed in terms of the parameter PSENOB introduced in Ref. [1], with the addition of two correction terms that include any baseline- and finite-time-related effect. These parameters are reported for representative filters as a function of a normalized baseline time. The obtained results have been validated for various T_{BL} times and ADC parameters by comparing them with a realistic simulation—a high-resolution germanium detector in a wide dynamic-range configuration. The ADC non-linearities effects have been also briefly considered.

These results have been confirmed by two experimental tests, using a germanium detector and a $\Delta E - E$ Silicon–CsI(Tl) telescope. For the first case, a low sensitivity to counting rate effects has been experimentally verified.

This work shows how to calculate the key parameters that, in practical applications, determine the resolution loss due to finite-time shaping and baseline subtraction. Besides, these effects are demonstrated to be negligible as soon as the used baseline time is of the order of twice the detector noise corner time. In this hypothesis, the system performances can be directly predicted using the simpler recipe of the companion paper [1].

Acknowledgments

The authors would like to thank D. Bazzacco, M. Bini, G. Pasquali, and N. Taccetti for interesting discussions, and M. Carlà for helpful suggestions about the ADC characterization measurements.

Appendix A. Comparison with the formalism of previous works

In this Appendix the shaping baseline subtraction method discussed in the paper is re-expressed using the formalism of Ref. [18].[3]

Whereas in this work all the signal processing has been formulated at the preamplifier level, in Ref. [18] only

[3] In this Appendix the definition of all the considered quantities is the same of the previous sections (Section 3). At variance with Ref. [18], where the time conventionally chosen as $t = 0$ corresponds to the arrival of the detector event, in this Appendix a time offset consistent with the one of the previous discussions (see for example Fig. 3) will be used, i.e. the detector event is placed at $t = T_{BL}$. This corresponds to a simple time shift of T_{BL} of the obtained weight functions with respect to Ref. [18].

quantities at the detector level are considered. Given the known preamplifier response $P(t)$ to a δ-like detector current, it is obviously possible to translate any signal processing algorithm from one formalism to the other. Although the preamplifier response $P(t)$ is not explicitly present in the equations of Ref. [18] (here resides one of the main advantages of that formalism) its detailed knowledge is needed in all practical applications of the method.

In Ref. [18] the shaping algorithm is mathematically represented as a weighted sum of the detector current $i(t)$, evaluated at the peaking time of the used filter. The weight function $W(t)$ is optimized in order to obtain the best SNR and to satisfy few constraints, including having a finite width. In this work the baseline is instead evaluated at the preamplifier level over a finite time T_{BL}. Nevertheless, the presence of the long preamplifier response (for example having an exponential decay) introduces a long-time correlation between the acquired samples $S[k]$, i.e. the weight function $W(t)$ develops over a time much longer than T_{BL}—over an infinite time if $P(t)$ has an infinite length.

Carrying out the computations, recalling that both $P(t) = G(t) = 0\ \forall t<0$, the (non-normalized) weight function of the method used in this work is given by

$$W(t) = \int_0^{T_{B+M}} P(\tau - t)G(T_{B+M} - \tau)\,d\tau - \frac{1}{T_{BL}}\left[\int_0^{T_{BL}} P(\tau - t)\,d\tau\right] \times \left[\int_0^{T_{B+M}} G(T_{B+M} - \tau)\,d\tau\right] \quad (A.1)$$

valid for $-\infty<t<T_{B+M}$. It is easily seen that $\int_{-\infty}^{T_{B+M}} W(t)\,dt \equiv 0$ for any P, G functions and T_{BL} time,

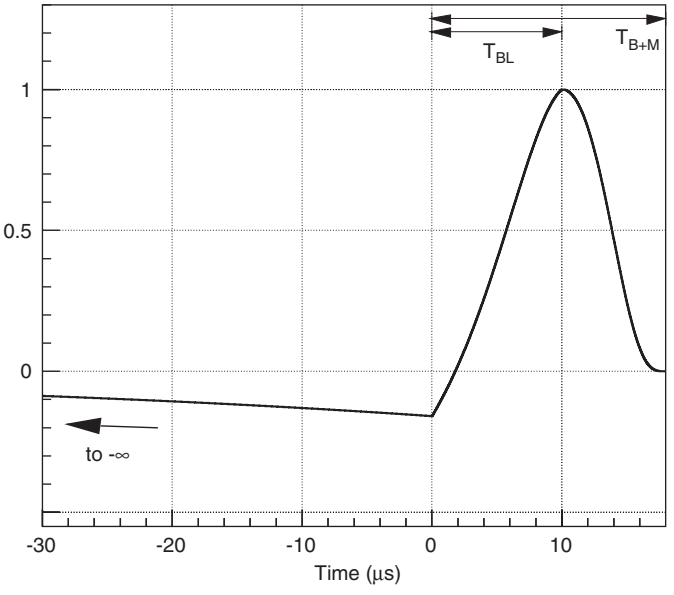

Fig. A.1. Weight function (as defined in Ref. [18]) for the baseline subtraction method used in this work. A configuration similar to the experiment described in Section 7.1 has been used, see text for details.

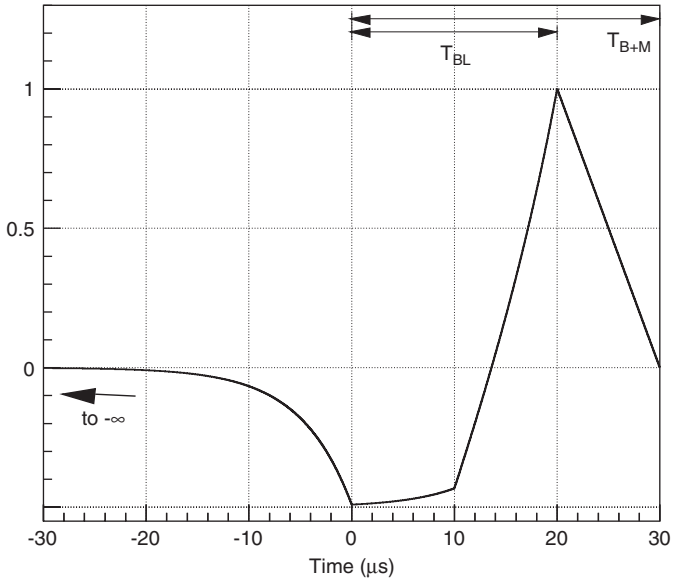

Fig. A.2. As Fig. A.1, but using an experimental arrangement similar to Ref. [22], see text for details.

i.e. $W(t)$ is "area balanced". As discussed in Ref. [18], this property of the weight function ensures a perfect elimination of any baseline DC offset. This behaviour of the used baseline subtraction method was already discussed from a different point of view in Section 3.

In Figs. A.1 and A.2 two examples of $W(t)$ as computed with Eq. (A.1) are reported. In Fig. A.1 $W(t)$ for the configuration used in Section 7.1 is shown (2 μs CR-RC^4 shaping, 10 μs baseline, 50 μs preamplifier decay time), whereas in Fig. A.2 an example of $W(t)$ obtained applying the baseline subtraction method of this work to an experimental setup similar to Ref. [22] is shown (10 μs triangular shaping, 20 μs baseline, 5 μs preamplifier decay time). The comparison of the obtained weight functions with the ones of Ref. [18] shows that a qualitative agreement exists between the method proposed in this work and the one of Ref. [18], although no noise optimization has been performed in this work. This result is not surprising because, although non-optimal, the used baseline subtraction and shaping method is able to provide spectroscopy-grade resolutions, and thus the weight function is expected not to be dramatically different from the one used in the optimal system.

Appendix B. Expressions for k_G and h_G

In this Appendix explicit expressions for $k_G(T_{BL})$ and $h_G(T_{BL})$, used in Section 4 are given. These are the expression used to extract the numerical values shown in Section 4.

k_G By substituting into Eq. (7) the white noise autocorrelation function (i.e. a δ-function) one

obtains

$$k_G^2(T_{BL}) = \frac{1}{2}\int_0^{T_{B+M}} [G(x)]^2\,dx + \frac{1}{T_{BL}}\,G_{int}(T_{B+M}) \times\left[1-\frac{1}{2}\,G_{int}(T_{B+M})\right] \quad (B.1)$$

where, in analogy with Ref. [1], the normalization $G_{int}(T_M)=1$ has been used.

h_G Since the autocorrelation function of a spectral noise density a/ω^2+b cannot be computed (it diverges due to low frequency terms), a direct application of Eq. (7) is not possible. This is due to the mathematical assumption of having a preamplifier with an infinite decay time, i.e. a perfect integrator. When the preamplifier decay time τ_{pre} is taken into account and $\tau_{pre} \gg \sqrt{b/a}$, the following spectral noise density can be written:

$$w(\omega) = a\cdot\frac{\tau_{pre}^2}{1+\tau_{pre}^2\omega^2} + b. \quad (B.2)$$

The non-white term is now characterized by a finite autocorrelation function. By applying Eq. (7), and performing the limit $\tau_{pre}\to\infty$ in order to recover the desired a/ω^2+b schematization, one obtains

$$\begin{aligned} h_G^2(T_{BL}) &= \frac{1}{2}\int_0^{T_{B+M}} [G_{int}(x)]^2\,dx \\ &\quad -\frac{1}{2}\,G_{int}(T_{B+M})\int_0^{T_{B+M}} G_{int}(x)\,dx \\ &\quad -\frac{T_{BL}}{12}\,[G_{int}(T_{B+M})]^2 + \frac{G_{int}(T_{B+M})}{4T_{BL}} \\ &\quad \times\left\{\int_0^{T_{B+M}} [(T_{B+M}-x)^2 + (T_M-x)^2] \right. \\ &\quad \left. \times G(x)\,dx - 2\int_{T_M}^{T_{B+M}} (T_M-x)^2 G(x)\,dx\right\}. \end{aligned} \quad (B.3)$$

$k_{G\star}$,$h_{G\star}$ The quantities $k_{G\star}$ and $h_{G\star}$ are defined in analogy with k_G, h_G but for the adimensional variables $x_{B+M}=T_{B+M}/\vartheta$, $x_{BL}=T_{BL}/\vartheta$ and the adimensional functions $G^\star(t)$ and $G_{int}^\star(t)$. They can be immediately computed starting from Eq. (B.1) and Eq. (B.3). $k_{G\star}$ and $h_{G\star}$ are adimensional variables, related to k_G and h_G by $k_G^2 = k_{G\star}^2/\vartheta$, $h_G^2 = h_{G\star}^2\vartheta$, respectively. In Section 4 the parameter ϑ has been chosen as $\tau_{C,opt}$.

References

[1] L. Bardelli, G. Poggi, Digital sampling-systems in high-resolution and wide dynamic-range energy measurements: comparison with peak sensing ADCs, this issue.
[2] E. Gatti, et al., Nucl. Instr. and Meth. A 523 (2004) 167.
[3] L. Bardelli, et al., Nucl. Instr. and Meth. A 491 (2002) 244.
[4] W. Gast, et al., IEEE Trans. Nucl. Sci. NS-48 (6) (2001) 2380.
[5] G. Pasquali, et al., in preparation;
G. Pasquali, et al., A DSP-equipped digitizer for online analysis of detector signals, IWM 2005 Workshop, Catania (CT) Novermber 28th–December 1st 2005.
[6] Technical proposal for the Advanced GAmma Tracking Array (AGATA) project, available on ⟨http://agata.pd.infn.it/⟩.
[7] M.A. Deleplanque, et al., Nucl. Instr. and Meth. A 430 (1999) 292.
[8] L. Bardelli, et al., Nucl. Instr. and Meth. A 521 (2004) 480.
[9] L. Bardelli, et al., Proceedings of RNB6 conference, 2003, Nucl. Phys. A 746 (2004) 272.
[10] L. Bardelli, et al., in: G. La Rana, C. Signorini, S. Shimoura (Eds.), Proceedings of the Fifth Italy–Japan Meeting, Naples, Italy, 3–7 November 2004, World Scientific 2006, ISBN-981-256-523-X.
[11] J. Pouthas, et al., Nucl. Instr. and Meth. A 357 (1995) 418.
[12] G. Casini, et al., Eur. Phys. J. A 9 (2000) 491.
[13] S. Piantelli, et al., Phys. Rev. Lett. 88 (2002) 052701.
[14] M. Bini, et al., Nucl. Instr. and Meth. A 515 (2003) 497.
[15] F. Gramegna, et al., Nucl. Instr. and Meth. A 389 (1997) 474.
[16] S. Aiello, et al., Nucl. Phys. A 583 (1995) 331c.
[17] V. Radeka, Rev. Sci. Instr. 38 (1967) 1397.
[18] A. Pullia, G. Ripamonti, Nucl. Instr. and Meth. A 376 (1996) 82.
[19] R.E. Chrien, R.J. Sutter, Nucl. Instr. and Meth. A 249 (1986) 421.
[20] F.S. Goulding, Nucl. Instr. and Meth. 100 (1972) 493.
[21] A.V. Oppenheim, R.W. Shafer, Digital Signal Processing, Prentice-Hall, Englewood Cliffs, NJ, 1975.
[22] A. Pullia, A. Geraci, G. Ripamonti, Nucl. Instr. and Meth. A 439 (2000) 378.
[23] L. Bardelli, et al., Application of a fast digital sampling system to $\Delta E - E$ identification and subnanosecond timing, Laboratori Nazionali di Legnaro, Annual Report, 2002.
[24] R.A. Winyard, J.E. Lutkin, G.W. McBeth, Nucl. Instr. and Meth. 95 (1971) 141.
[25] M. Alderighi, et al., IEEE Trans. Nucl. Sci. NS-51 (4) (2004) 1475.